Understanding Nonequilibrium Solute and Solvent Motions through Molecular Projections: Computer Simulations of Solvation Dynamics in Liquid Tetrahydrofuran (THF)

Michael J. Bedard-Hearn, Ross E. Larsen, and Benjamin J. Schwartz*

Department of Chemistry and Biochemistry, University of California, Los Angeles California,
607 Charles E. Young Drive East, Los Angeles, California 90095-1569

Received: June 27, 2003; In Final Form: September 30, 2003

In this paper, we investigate the solvation dynamics of the weakly polar organic solvent tetrahydrofuran (THF) via classical molecular dynamics simulation. We find that the relaxation dynamics of all of the rotational and translational degrees of freedom of neat THF occur on similar time scales and have similar power spectra, making it impossible to use spectral density analysis to discern which specific molecular motions are involved in solvation. Instead, we probe the molecular origins of solvation dynamics using a nonequilibrium projection formalism that we originally outlined in M. J. Bedard-Hearn et al., *J. Phys. Chem. A* **2003**, *107* (24), 4773. Here, we expand this formalism and use it to study the nonequilibrium solvation dynamics for a model reaction in THF in which a charge is removed from an anionic Lennard-Jones (LJ) solute, leaving behind a smaller neutral atom. The solute parameters are chosen to model the photodetachment of an electron from a sodium anion, $Na^- \rightarrow Na^0$, to compare to the results of ultrafast spectroscopic experiments of this reaction being performed in our lab. We are able to explain the hidden breakdown of linear response for this system that we uncovered in our previous work in terms of the dynamical properties of the neat liquid and the structural properties of the solutions. In particular, our nonequilibrium projection analysis shows that four distinct solvation mechanisms are operative: (1) a rapid relaxation ($t \leq 700$ fs) caused by longitudinal translational motions that dramatically change the local solvation structure; (2) a slower relaxation ($t > 700$ fs) caused by diffusive longitudinal translational motions that completes the transformation of the long-range solute–solvent packing; (3) an early-time relaxation ($t < 500$ fs) caused by solvent rotational motions that destabilizes the (unoccupied) anion ground state via Coulomb interactions; (4) a longer time process ($t \geq 500$ fs) caused by solvent rotational motions that *increases* the solvation energy gap. This last process results from the LJ interaction component of the solvent rotational motions, as the nonequilibrium dynamics bring smaller THF–oxygen sites closer to the excited solute in place of larger THF–methylene sites. Overall, the simulations indicate that nonequilibrium solvation dynamics involves cooperative motions of both the solute and solvent and consists of multiple competing relaxation processes that can affect the solvation energy gap in opposite directions.

I. Introduction

Tetrahydrofuran (THF) is an important organic solvent employed extensively in synthesis and commonly used in spectroscopic studies. Despite the importance of this solvent, there have been surprisingly few computer simulations aimed at understanding the dynamical solvation properties of THF on the molecular level. Jorgensen and co-workers developed a united atom (5-site) model for THF, and performed Monte Carlo (MC) calculations to explore the static structural properties of both neat THF and of a sodium cation dissolved in THF.[1,2] These researchers found that the disk-like THF molecules tend to arrange in parallel-ring structures, or short chains, in the neat fluid, and that they form a near-square-pyramidal structure around Na^+.[2] Jorgensen and co-workers also explored the effects of puckering of the THF ring and concluded that nonplanarity or psuedorotation of the ring makes little difference to the equilibrium structure of this fluid.[1]

In addition to Jorgenson's MC-based structural studies, there have been a few limited computational studies of the dynamical properties of THF; we are aware of only four such investigations in the literature. The first, by Drabowicz, used Jorgensen's

model in molecular dynamics (MD) simulations,[3] although Drabowicz calculated a radial distribution function (RDF) with a slightly different first peak position than Jorgensen's. In addition to the RDF, Drabowicz calculated the THF center-of-mass and angular velocity autocorrelation functions. A second MD study took advantage of Jorgenson's model but reported only the diffusion constant.[4] The authors in this study had removed the partial charges (and therefore the dipole moment) from the THF molecules in their calculation, so it is unclear whether their reported diffusion constant is relevant to either the simulated or experimental fluid.[4] The third MD study, by Helfrich and Hentschke, simulated segments of a polymeric residue in liquid THF.[5] As part of this study, the authors developed their own model for THF using a packaged software program (AMBER), choosing their parameters to obtain a diffusion constant that was as close as possible to the experimental value. Thus, Helfich and Hentchke's model used very different parameters than Jorgensen's. In their conclusions, Helfrich and Hentschke noted only that the high symmetry of THF seemed to lead to a pronounced solvent structure; these authors did not calculate any dynamical quantities other than the diffusion constant. Finally, and most recently, there has been a series of publications by Müller-Plathe and co-workers exploring the uniqueness of the MD simulation parameters when

---

* Corresponding author. E-mail: schwartz@chem.ucla.edu. Fax: (310) 206-4038. Voice: (310) 206-4113.

SCHEME 1
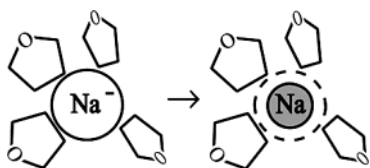
attempting to simulate a specific experimental solvent.[6] These workers used a variety of different force field parameters to model THF and calculated some thermodynamic properties and the diffusion constant for each model. However, none of these previous MD or MC calculations has provided the level of analysis of THF needed to understand the dynamical behavior of this important organic solvent.

Our interest in the dynamical properties of THF stems from recent ultrafast spectroscopic studies in our lab investigating charge-transfer-to-solvent (CTTS) reactions in this solvent.[7] Our experiments have focused on the dynamics of the photodetachment of electrons via CTTS excitation of sodium anions (Scheme 1). Because the sodium anion CTTS system has only electronic degrees of freedom (the reactants and products are either single atoms or solvated electrons), the charge transfer dynamics are determined solely by the motions of the sodium atom and the surrounding THF solvent molecules.[7] Thus, the purpose of this paper is to gain better insight into the dynamical properties of THF as a solvent via MD simulation. In the results presented below, we will investigate both the properties of the equilibrium fluid and the nonequilibrium solvation dynamics resulting from the ionization of a sodide-like solute in THF.

The chief quantity of interest in solvation dynamics is the solvation energy gap, $\Delta E = E^{exc} - E^{gnd}$, where E^{exc} and E^{gnd} are the solute−solvent interaction energies when the solute is in the excited and ground states, respectively. The normalized nonequilibrium solvent response function, $S(t)$, is defined by[8]

$$S(t) = \frac{\overline{\Delta E}(\mathbf{R};t) - \overline{\Delta E}(\mathbf{R};\infty)}{\overline{\Delta E}(\mathbf{R};0) - \overline{\Delta E}(\mathbf{R};\infty)} \qquad (1)$$

where $\mathbf{R}$ denotes the positions of the solute and all of the solvent molecules and the overbar represents a nonequilibrium ensemble average in which the solute is promoted to its excited state at $t = 0$. Equation 1 is normalized to begin at 1 and decay to 0 after the system has equilibrated around the excited-state solute. Thus, $S(t)$ determines the rate at which the solute and solvent relax to accommodate changes in the electronic or structural properties of the solute resulting from excitation. Experimentally, $S(t)$ is assumed to be simply related to the relaxation time scales observed in time-resolved fluorescence (Stokes shift)[8,9] or photon echo spectroscopies.[10]

One of the primary tools used to study solvation dynamics is the idea of linear response (LR), which is based on the Onsager regression hypothesis.[11] In the LR limit, $S(t)$ is equivalent to the equilibrium solvation time correlation function (TCF),[8,11]

$$C(t) = \frac{\langle \delta\Delta E(0)\, \delta\Delta E(t) \rangle}{\langle (\delta\Delta E)^2 \rangle} \qquad (2)$$

where the angled brackets denote an equilibrium ensemble average and $\delta\Delta E = \Delta E - \langle \Delta E \rangle$ is the equilibrium fluctuation of the energy gap (and the $\mathbf{R}$ dependence is repressed). The equilibrium solvation correlation function, $C(t)$, measures the persistence of memory of the energy gap. In the LR limit, the

motions of the solute and solvent molecules in response to a small perturbation that takes the system away from equilibrium are the same as those that follow from a natural equilibrium fluctuation of the energy gap; in this limit, one can show that $S(t) = C(t)$.[11] Experimentally, the dynamics of spectral diffusion measured in transient hole burning experiments is assumed to be simply related to $C(t)$.[12]

In most (but not all[13,14]) simulations of solvation dynamics in which the excited state of the solute involves a charge redistribution, $S(t)$ and $C(t)$ are found to agree, implying that most such systems fall within the limit of LR. However, LR is observed to fail when the excitation of the solute involves a change in size or shape.[14] This is because the change in solute volume upon excitation drives nearby solvent molecules into locations that they never explore at equilibrium (in the case of a size decrease) or excludes nearby solvent molecules from space that was formerly accessible at equilibrium (in the case of a size increase). This means that when size changes are included, the solvent samples a different configuration space at equilibrium than it does away from equilibrium; therefore, the equilibrium and nonequilibrium relaxation dynamics need not be the same.

Of course, it is always possible that a situation arises where the equilibrium and nonequilibrium relaxation dynamics of a system are different but occur on similar time scales, so that $S(t)$ agrees with $C(t)$ by coincidence, but LR does not hold. In recent work, we presented a preliminary MD exploration of the LR approximation for a negatively charged solute in THF that undergoes the loss of its charge and a decrease in size (Scheme 1).[15] We found a rough agreement between $S(t)$ and $C(t)$ despite the fact that the simulated solute perturbation included a significant decrease in solute size. We then showed how to project the nonequilibrium solvation dynamics onto any molecular coordinate of the system,[15] and we compared these nonequilibrium projections to projections of the equilibrium dynamics[16,17] based on Steele theory.[18] We found that even though $S(t)$ agreed fairly well with $C(t)$ for this system, the solute and solvent motions underlying the relaxation dynamics for the equilibrium and nonequilibrium processes were completely different. We concluded that there was a hidden breakdown of LR for this solute−solvent system because it was not immediately obvious from the comparison of $S(t)$ and $C(t)$ that LR fails.

In this paper, we extend our analysis of the details underlying the dynamics of this particular solute−solvent system that exhibits a hidden breakdown of LR. We also present detailed analyses of both the dynamical properties of Jorgensen's model of THF and the nonequilibrium solvation dynamics of an atomic solute in this model of THF. In particular, we explore the relationship between the structural and dynamic equilibrium properties of THF and the mechanism of nonequilibrium solvation. We begin in section II by describing the computational methods used in our MD simulations, and then present the results of equilibrium simulations in section III. In section III.A, we show our results for neat THF and in section III.B, we discuss the equilibrium simulations of solutions of both sodium and sodide in THF. Section IV is divided into three parts: part A discusses the formalism we use to project the nonequilibrium solvation energy gap onto solute and solvent molecular degrees of freedom, part B presents the results of nonequilibrium MD simulations modeling the ionization of a sodide-like solute in THF (Scheme 1), and part C provides a molecular picture of the solvation dynamics in this model solute−solvent system. In section V, we address the reasons why LR breaks down in

TABLE 1: Lennard-Jones and Coulomb Potential Parameters for the Solute−Solvent Systems Studied in This Work (Eq 3)[a]

	σ (Å)	$\epsilon \times 10^{-21}$ (J)	q (e)
Oxygen	3.0	1.18	−0.5
α-methyl	3.905	0.82	+0.25
β-methyl	3.905	0.82	0.0
Na^0	3.14[b]	14.7	0.0
Na$^-$	5.21[c]	3.11[d]	−1.0

[a] All parameters taken from ref 1 unless otherwise noted. [b] Estimated from various sources. [c] Calculated from ref 23; see text for details. [d] Calculated from ref 24; see text for details.

the face of the seeming agreement between $S(t)$ and $C(t)$, and we offer some concluding remarks.

II. Computational Methodology

All of the simulations discussed in this paper consist of microcanonical (constant E, V, N) molecular dynamics (MD) simulations of an atomic (Lennard-Jones) solute and 255 THF solvent molecules (or 256 THF molecules for simulations of the neat solvent). The equations of motion were integrated using the Verlet algorithm[19] with a 1 fs time step. The simulation cell had a density of 0.8892 g/cm^3 (the same as the experimental fluid at 295 K), corresponding to a cubic simulation box 32.5 Å on a side. The system had an equilibrium temperature of ∼298 ± 5 K. In all cases the total energy was conserved to better than 0.001%.

The THF solvent molecules were modeled using the five-site (unified methylene groups) potential introduced by Jorgensen, which has partial charges on the oxygen and two α-methylene sites.[1] We used a modified SHAKE algorithm[20] to keep the molecules rigid and planar. The site−site interaction potentials in this model are a pairwise sum of Coulomb and Lennard-Jones terms, such that the interaction between any two sites, i and j is

$$u_{ij}(r_{ij}) = \frac{1}{4\pi\epsilon_0} \frac{q_i q_j}{r_{ij}} + 4\epsilon_{ij}\left[\left(\frac{\sigma_{ij}}{r_{ij}}\right)^{12} - \left(\frac{\sigma_{ij}}{r_{ij}}\right)^6\right] \quad (3)$$

where r_{ij} is the distance between the ith and jth sites, which could be any of the solvent sites or the Lennard-Jones solute; the solvent parameters of Jorgensen's model are listed in Table 1.[1] The site−site potentials of eq 3 were further modified by including a center-of-mass tapering function that smoothly brought the potential to zero over a distance of 0.5 Å with a final cutoff radius of 15.9 Å.[21,22] We found that when we used a site-based cutoff (either strict spherical or tapered) for the potential instead of the center-of-mass-based cutoff, the solvent unnaturally froze. Minimum image periodic boundary conditions[19] were used throughout the simulations except for the calculation of the diffusion constant.

For the solute, we chose potential parameters to model the conversion of a solvated sodium anion into a solvated neutral sodium atom, as a simple imitation of the femtosecond experiments studying charge-transfer-to-solvent reactions being performed in our lab.[7] All of the solute parameters also are listed in Table 1. For the excited-state solute (neutral), we used a sodium−sodium Lennard-Jones well depth of $\epsilon = 1.47 \times 10^{-20}$ J, and we estimated the size of the excited-state solute to be close to that of a sodium atom. For the ground-state (anion) solute, we used a sodide−sodide size based on the crystal structures of sodide salts obtained by Dye et. al.,[23] and we used Edwards' polarizability measurements[24] to estimate the sodide−sodide well depth. For the solute−solvent Lennard-Jones

interactions, we used the solute and solvent Lennard-Jones parameters listed in Table 1 and the standard Lorentz−Berthelot combining rules.[19] The ground-state solute also contained a charge of $-e$ that interacted by the Coulomb potential with the partial charges on the oxygen and α-methylenes of each THF solvent molecule.

Starting from an fcc lattice, we equilibrated the neat solvent and the solute−solvent systems with velocity rescaling for 5−10 ps, followed by at least 10 ps of additional equilibration. We then ran a neat solvent trajectory for 100 ps, and ran equilibrium solution simulations—one with the anionic solute and one with the neutral solute—for 200 ps each. We also ran 400 nonequilibrium trajectories, each of 12 ps duration. Because the nonequilibrium solvation dynamics were completed in only a few picoseconds, running to 12 ps allowed us to ensure that the system had fully equilibrated around the neutral excited state. The nonequilibrium simulations were started by choosing uncorrelated configurations[25] from the ground-state (anion) equilibrium run and instantly removing the charge and changing the Lennard-Jones parameters to those of the excited state (neutral). Each initial configuration provided the starting points for two nonequilibrium trajectories: one in which the velocities were kept unchanged, and another in which the velocities were reversed. To mimic a resonant absorption, the starting configurations were chosen by requiring the solvation energy gap, ΔE, to be within 0.75% of the equilibrium average. The temperature of the equilibrium solution simulations did not change noticeably from the neat solvent simulations, but the nonequilibrium calculations saw an increase in temperature of about 8 K following excitation of the solute.

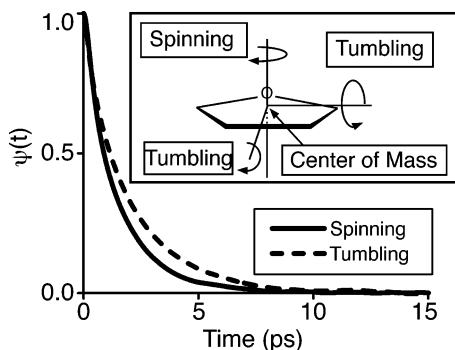## III. Equilibrium and Nonequilibrium Solvation Properties of THF

In this section, we set the stage for our exploration of the molecular motions involved in nonequilibrium solvation by first examining some of the equilibrium properties of both neat THF and THF solutions. We also present both equilibrium and nonequilibrium solvent response functions and we discuss the reasons why the LR approximation might be expected to break down following excitation of our atomic anion solute.

A. Equilibrium Structure and Dynamics of neat THF. The static structural and thermodynamic properties of this model of THF already have been explored in the MC simulations of Jorgenson and co-workers.[1,2] The advantage of MD over MC simulations, however, is that MD provides information about dynamic properties, such as time correlation functions and the diffusion coefficient. We begin by investigating one of the simplest equilibrium dynamical properties of the system, the rotational dynamics of the THF molecules, which are explored in Figures 1 and 2. Figure 1 shows the normalized orientation autocorrelation function

$$\psi(t) = \langle \hat{\mathbf{u}}(t) \cdot \hat{\mathbf{u}}(0) \rangle \quad (4)$$

for a unit vector, $\hat{\mathbf{u}}$, that lies either in the plane of the THF molecule, $\hat{\mathbf{u}}_s$ (spinning, solid curve), or perpendicular to the plane of the THF ring, $\hat{\mathbf{u}}_{t1}$ and $\hat{\mathbf{u}}_{t2}$ (tumbling, dashed curve, calculated as the sum of both tumbling rotations and tumbling cross-terms), as depicted in the inset to Figure 1.[26] The relaxation times for the orientation autocorrelation functions were $\tau_{\text{tumble}} = 1.9$ ps and $\tau_{\text{spin}} = 1.6$ ps, which we determined by fitting the curves to single exponential decays (not shown).[27]

Figure 2 shows the velocity autocorrelation (VAC) functions, $A(t)$, for the center-of-mass velocity (solid curve) and the angular velocities for the spinning (dotted curve) and the sum of the

Molecular Projections of Solute and Solvent Motions

J. Phys. Chem. B, Vol. 107, No. 51, 2003 **14467**

Figure 1. Equilibrium angular orientation autocorrelation functions, $\psi(t)$ (eq 4), showing the spinning (solid curve) and tumbling (dashed curve) degrees of freedom for neat THF. The inset shows the three rotational degrees of freedom for this model. The tumbling correlation function includes both tumbling directions and the tumbling-tumbling cross term.
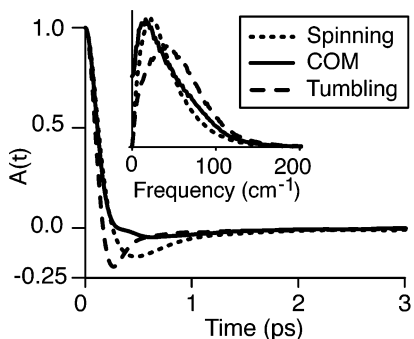

Figure 2. Equilibrium velocity autocorrelation functions (VACs), $A(t)$ (eq 5), for neat THF. The spinning (dotted curve) and tumbling (dashed curve) motions are defined as in the inset to Figure 1. The inset shows the power spectrum for each of the VACs, indicating that the center-of-mass translations (COM, solid curve) and spinning and tumbling rotations span similar frequency ranges.

tumbling (dashed curve) degrees of freedom. The VACs were calculated using

$$A(t) = \frac{\langle \dot{\mathbf{u}}(t) \cdot \dot{\mathbf{u}}(0) \rangle}{\langle \dot{\mathbf{u}}^2 \rangle} \qquad (5)$$

where $\dot{\mathbf{u}}(t)$ is either the center-of-mass velocity, or the spinning or tumbling angular velocities.[16b,28] Although the orientation autocorrelation functions decay on the $\sim$1–2 ps time scale, all of the VACs have $1/e$ decay times of $\sim$0.25 ps. We note that in the MD calculations by Drabowicz,[3] the time ordering of the center-of-mass and angular velocity time correlation functions is reversed from what we show in Figure 2. We believe that this may be the result of an incorrect labeling of the curves in Figure 4 of ref 3. The featureless relaxation of the VACs in Figure 2 is similar to that observed for other weakly polar planar molecules, such as benzene.[29] We believe that the slow relaxation of the orientational time correlation functions is the result of steric hindrance due to packing of the solvent molecules; the solvent VACs all show a significant negative region, indicating that THF has limited mobility due to strong solvent caging.

The inset to Figure 2 shows the power spectrum for each of the velocity autocorrelation functions, all of which are characterized by a large broad band between 0 and 200 cm^{-1}. Thus, not only does the memory of molecular rotations and translations persist for similar times, but the underlying motions occur in similar frequency ranges. This makes it nearly impossible to distinguish the solvent motions that are involved in solvation
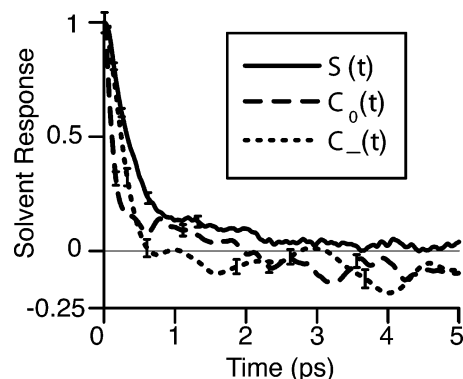
Figure 3. Solvent response functions for different sodium and sodide simulations in THF. $S(t)$ (solid curve, eq 1) is the nonequilibrium response when the anion is instantly changed into the neutral (see Scheme 1), calculated from 400 nonequilibrium trajectories. $C_0(t)$ (dashed curve, eq 2) is the equilibrium solvation response when the solute is neutral sodium and the unoccupied solute state is the anion. $C_-(t)$ (dotted curve, eq 2) is the equilibrium solvation response when the solute is the anion the unoccupied excited-state solute is the neutral. Both equilibrium solvent response functions were calculated from 200 ps trajectories. The error bars shown are two standard deviations.[30]

by their time scale or by spectral density analysis.[14,28] It is for this reason that we have elected to explicitly project the dynamics of specific solvent motions, as detailed below in section IV.A.

Finally, to close our exploration of the equilibrium dynamical properties of this model of THF, we have calculated the value of the self-diffusion constant using the Einstein equation[19] for the mean-square displacement of the center of mass, $6Dt = \langle |\mathbf{r}(t) - \mathbf{r}(0)| \rangle^2$, where $\mathbf{r}(t)$ is the position of the center of mass at time t. The experimental diffusion coefficient, $D_{\exp} = 3.5 \times 10^{-5}$ cm^2/s,[5] is somewhat higher than the one we calculated for this model, $D = 2.88 \times 10^{-5}$ cm^2/s, suggesting that Jorgensen's model may overestimate the tendency of this solvent to stack and cluster.

B. Solvation Dynamics and the Equilibrium Structure of Atomic Solutes in THF. In this section, we discuss the dynamical properties of solutions containing an anionic or neutral atomic solute. In the LR approximation, the solute–solvent interactions are characterized by the equilibrium solvation response function $C(t)$, eq 2. Figure 3 shows the equilibrium solvent response for the anionic solute ($C_-(t)$, dotted curve), which is the ground state for the nonequilibrium simulations, and the equilibrium solvent response for the neutral solute ($C_0(t)$, dashed curve), which will be the excited state for the nonequilibrium simulations.[30] The solvation energies of the unoccupied excited states were calculated using the neutral solute interaction parameters for $C_-(t)$ and the anionic solute interaction parameters for $C_0(t)$. Also shown in Figure 3 is the nonequilibrium solvent response, $S(t)$ (solid curve, eq 1), calculated from 400 nonequilibrium trajectories in which the solute simulation parameters were switched from those of the anion to those of the neutral, mimicking electron photodetachment from a sodium anion. In the limit of LR, we would expect the equilibrium solvation time correlation functions for the anion and neutral simulations to be the same. Because the two equilibrium response functions are clearly different, we anticipate that LR will break down for the nonequilibrium perturbation that converts the anionic solute into the neutral solute.

At the earliest times, $S(t)$ and $C_-(t)$ are almost identical, although there are small deviations at later times. (In fact, the differences between $C_-(t)$ and $C_0(t)$ would not ordinarily deter us from invoking the LR approximation given how similar the

TABLE 2: Properties of the Equilibrium (Eqb) and Nonequilibrium (Neqb) Solvation Response Functions, as Well as the Structural Properties of the Anion (Ground State) and Neutral (Excited State) Solutions at Equilibrium[a]

	τ, fs	$\langle E_{ss}\rangle$,[b] kT	solvation energy, $k_B T$	$\langle \Delta E\rangle_\eta$,[c] $k_B T$	$g_{0-com}(r)$,[d] Å	$g_{0-oxy}(r)$,[d] Å
(Eqb)Anion	135 ± 17^e	~ 90	$\sim 1^f$	$\sim 75^g$	5.7	6.3
(Eqb)Neutral	63 ± 6^e	~ 15	$\sim 45^f$	~ 105	4.7	3.8
(Neqb)Na$^-$ → Na^0	259^h	n/a	$\sim 180^i$	n/a	n/a	n/a

[a] All equilibrium quantities were calculated from 200 ps simulations. The nonequilibrium data were calculated from the 400 trajectories, each of 12 ps duration. [b] The average solute−solvent interaction energy, as defined as in the text. [c] The average equilibrium energy gaps, $\langle \Delta E\rangle_\eta = \langle E^{anion} - E^{neutral}\rangle_\eta = \langle E^{anion}\rangle_\eta - \langle E^{neutral}\rangle_\eta$, for the simulations with the anionic solute and neutral solute. $\langle E^{anion}\rangle$ is the average anion solute−solvent interaction energy, $\langle E^{neutral}\rangle$ is the average neutral solute−solvent interaction energy, and η indicates whether the equilibrium dynamics were performed with the neutral or anionic solute. [d] First peak distance for the solute−solvent center-of-mass (0-com) or solute−solvent oxygen site (0-oxy) radial distribution function. [e] Calculated from a 200-ps trajectory as $\tau^{-2} = -d^2 C(0)/dt^2 = -G(0)/\langle \delta \Delta E^2\rangle$ (see ref 16a); the error is 2 standard deviations. [f] The solvation energy for the equilibrium simulations is the root-mean-square of the average fluctuations of the energy gap, $\langle \delta \Delta E^2\rangle^{1/2}$. [g] The average energy gap for the ground state (anion) corresponds to the average energy of the perturbation in the nonequilibrium trajectories. In an experiment, this would be the excitation energy. [h] Calculated by fitting the first 30 fs of $S(t)$ to a parabola and using $\tau^{-2} = -d^2 S(0)/dt^2$. The error we report is for the parabolic fit, $R^2 = 0.9995$. [i] The solvation energy for the nonequilibrium simulations, $2\lambda = \overline{\Delta E}(0) - \overline{\Delta E}(\infty)$ is the Stokes shift energy; see text.

nonequilibrium solvation response, $S(t)$, is to $C_-(t)$.) The fact that $S(t)$ and $C_-(t)$ agree at early times is what might be predicted from LR. This is because immediately after excitation of the solute, the inertial solvent motions are expected not to change from those when the solute was still in its ground state. On the other hand, at longer times the solvent is approaching equilibrium around the excited-state (neutral) solute, so the long-time behavior of $S(t)$ should resemble $C_0(t)$ rather than $C_-(t)$.[8,9a] In a previous paper, however, we showed using the method of projections (see section IV.A, below) that the solute and solvent motions underlying $S(t)$ and $C_-(t)$ are completely different, including at the earliest times where the inertial dynamics are expected to be similar. In particular, we found that the inertial part of the equilibrium response, $C_-(t)$, was predominantly composed of solvent rotational motions, whereas the inertial part of the nonequilibrium relaxation, $S(t)$, resulted almost entirely from solute−solvent center-of-mass translations.[15] The characteristic inertial solvation times for each of the response functions shown in Figure 3 are summarized in Table 2.

Table 2 also summarizes the average solvation energies and the average solvation energy gaps, $\langle \Delta E\rangle_\eta = \langle E^{anion} - E^{neutral}\rangle_\eta$, for each of the equilibrium simulations, where η = anion (neutral) indicates dynamic calculations involving the anionic (neutral) solute. Note that our nonequilibrium trajectories were launched from starting configurations chosen so that the $t = 0$ nonequilibrium energy gap was within 0.75% of the average energy gap for the anion-solute system; that is, $\langle \Delta E\rangle_{anion} \cong \overline{\Delta E}(0)$. Table 2 also compares the root-mean-square equilibrium energy gap fluctuations $\langle \delta \Delta E^2\rangle^{1/2}$ to the total nonequilibrium energy relaxation (Stokes' shift), $2\lambda = \overline{\Delta E}(0) - \overline{\Delta E}(\infty)$, where λ is known as the solvent reorganization energy. In the limit of linear response, we would expect the nonequilibrium Stokes' shift to be proportional to the magnitude of the typical equilibrium fluctuations of the solute−solvent energy gap, $\langle \delta \Delta E^2\rangle$,[31]

$$\langle \delta \Delta E^2\rangle = 2\lambda k_B T \qquad (6)$$

The fact that the nonequilibrium relaxation is so much larger than what would be expected from the size of the anionic solute equilibrium fluctuations provides another indication that LR should fail, making the apparent agreement of $S(t)$ and $C_-(t)$ in Figure 3a all the more surprising.

As we will show below, it is possible to understand both the coincidental agreement between $S(t)$ and $C_-(t)$ and many of the details of solvation dynamics in THF in terms of the local solute−solvent structure. Therefore, we present solute−solvent
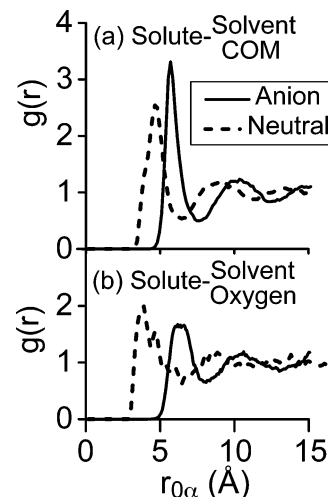
Figure 4. Equilibrium solute−solvent radial distribution functions for the anionic (solid curves) and neutral (dashed curves) solutes. (a) shows the solute−solvent center-of-mass distributions and (b) shows the solute−solvent oxygen site distributions. The first peak distances are summarized in Table 2.

radial distribution functions (RDF),[32] $g(r_{0\alpha})$, which give the probability of finding a solvent molecule (or site) α at a given distance from the solute (denoted by 0) in Figure 4. Panel a shows the solute−solvent center-of-mass RDFs for both the ground- (anion, solid curves) and excited-state (neutral, dashed curves) solutes, and panel b shows the corresponding solute−solvent oxygen site RDFs; the distances for all of the first-shell solvent peaks are listed in Table 2. Figure 4 makes it clear that the ground- and excited-state solutes impose very different local solvent structures; in fact, the different solute sizes lead to more THF molecules packed around the anion ($\sim$12 or 13) than around the neutral solute ($\sim$8 or 9). The large difference in first-shell distances is consistent with our previous paper,[15] where we concluded that center-of-mass translations contribute significantly to the nonequilibrium solvation dynamics.

Although the significant reorganization of solvent molecules (when the solute switches from anion to neutral) explains why translations dominate the nonequilibrium solvation response, this reorganization also allows us to rationalize why translational motions contribute so little to the solvation dynamics in $C_-(t)$.[15] The influence of solute or solvent fluctuations on the solvation energy gap not only comes from modulation of the occupied state but also results from modulation of the unoccupied state (in the case of the anionic solute, the unoccupied state is the small neutral atom). Typically, large fluctuations of the energy gap occur only if a particular solute or solvent motion causes

Molecular Projections of Solute and Solvent Motions

J. Phys. Chem. B, Vol. 107, No. 51, 2003 **14469**
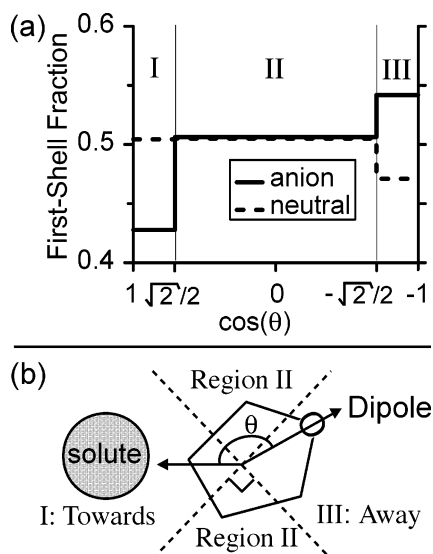
Figure 5. (a) Equilibrium angular distribution functions for the neutral (dashed curve) and anionic (solid curve) solutes. The area under each histogram is normalized to the number of solvent molecules (~12 for the neutral solute, ~13 for the anionic solute) within 7.5 Å of each solute.[49] We have binned the THF dipole orientations to lie within one of three regions defined by the dashed lines in (b): pointing in a 90° cone toward the solute (region I); pointing tangential to the solute (region II), or pointing in a 90° cone away from the solute (region III).

the energy of the ground and excited states to fluctuate in opposite directions. For our solute, the ground-state anion is so large that solvent molecules cannot translate close enough to modulate the energy of the unoccupied neutral excited state. Therefore, translation-based fluctuations cannot couple strongly to the solvation energy gap. This also means that all fluctuations of the energy gap are effectively fluctuations of only the anion solvation energy, and at equilibrium these fluctuations must have a magnitude of $\sim k_B T$. As it turns out, the equilibrium solvent motions that most strongly modulate the energy of the anionic solute are rotations that reorient the THF dipole.[15]

Finally, before turning to the molecular details of the nonequilibrium solvent relaxation, we note that Jorgensen and co-workers have studied the thermodynamics and equilibrium packing of THF around a charged Lennard-Jones particle that modeled a sodium cation.[2] By studying the solute−solvent interaction energies and solute−solvent RDFs, Jorgenson and co-workers discovered that the first-shell THF molecules interact very strongly with sodium cations, which impose a rigid local solvent structure with the THF oxygen atoms pointing toward the cation. In contrast, this type of rigid imposition of solvent orientational order does not occur with either our anionic or neutral solute. This is demonstrated in Figure 5a, which displays angular distributions of the first-shell[33] solvent dipoles around the ground- (anion, solid lines) and excited-state (neutral, dashed lines) solutes. Our geometry convention is illustrated in Figure 5b, with θ defined as the angle between the solvent dipole and the vector pointing from the solute to the solvent center-of-mass. In particular, we see that the distribution of solvent dipoles around the neutral solute is essentially uniform, whereas the distribution of solvent dipoles around the anion shows a small amount of local order, with a slight preference for the negatively charged THF oxygen site to point away from the anionic solute. On average, this amounts to less than one additional first-shell THF oxygen site pointing toward the neutral than pointing toward the anion. This detail turns out to be important in understanding the nonequilibrium solvation dynamics of this solute−solvent system, as we will discuss below in section IV.B.

IV. Nonequilibrium Solvation Dynamics of the Na⁻ → Na⁰ Reaction in THF

In this section, we review our new method for projecting out the contributions of different solute and solvent molecular motions onto the solvation energy gap. We then use these projections to explore the molecular details of nonequilibrium solvation dynamics in THF, with an eye toward building a molecular understanding of why LR breaks down for this solute−solvent system despite the apparent similarity of the equilibrium and nonequilibrium solvent response functions.

A. Method for Nonequilibrium Molecular Projections. In previous work, we were able to uncover the hidden breakdown of LR for our solute−solvent system by directly comparing the motions responsible for equilibrium and nonequilibrium solvation dynamics in $C_-(t)$ and $S(t)$.[15] To determine how specific molecular motions coupled to the equilibrium solvation energy gap, we used Steele theory,[16,18] and we developed a new formalism to project the contribution from any degree of freedom onto the nonequilibrium solvation energy gap.[15] Finally, we presented a new way to analyze the dynamics underlying $C(t)$ and $S(t)$ by integrating the projected derivatives, providing both a direct measure of the magnitude of the coupling between a solute or solvent degree of freedom and the solvation energy gap and a means for extracting the time scale for relaxation of that degree of freedom.[15] Here, we briefly review our method for projecting the molecular contributions to nonequilibrium solvation dynamics.

Using the chain rule for differentiation, we can write the rate of change of the total solvation energy gap, ΔE, as

$$\Delta \dot{E} = \sum_{\alpha} \frac{d\alpha}{dt} \frac{\partial \Delta E}{\partial \alpha} = \sum_{\alpha} \Delta \dot{E}_{\alpha} \equiv \sum_{\alpha} J_{\alpha}(t) \tag{7}$$

where the sum on α runs over all degrees of freedom, the over-dot denotes a derivative with respect to time, and we have defined $J_{\alpha}(t)$ as the velocity projection onto α. For equilibrium solvation dynamics, molecular information is contained in the solvation velocity TCF,

$$G(t) = \sum_{\alpha} \sum_{\beta} \langle \Delta \dot{E}_{\alpha}(t) \cdot \Delta \dot{E}_{\beta}(0) \rangle = \sum_{\alpha} \sum_{\beta} -\ddot{C}_{\alpha\beta}(t) \tag{8}$$

By integrating eq 8 twice with respect to time, the contributions from the degrees of freedom α and β, $C_{\alpha\beta}(t)$, to the equilibrium solvation TCF (eq 2) can be explored separately. This type of analysis has been used to study how molecular rotations, translations, and rotation/translation coupling drive equilibrium solvation dynamics in both polar and nondipolar solvents.[16,17]

To investigate the molecular contributions to nonequilibrium solvation dynamics, we rewrite the total nonequilibrium solvation velocity response function, $J(t)$ (eq 7), in terms of a specific complete set of projections: the solute and solvent site Cartesian coordinates. Thus

$$J(t) = \sum_{\mu} \overline{\Delta \dot{E}}(R_{\mu 0}; t) = \sum_{\mu} [\dot{\mathbf{R}}_{\mu} \cdot \hat{\mathbf{R}}_{\mu 0} - \dot{\mathbf{r}}_0 \cdot \hat{\mathbf{R}}_{\mu 0}] \Delta E'(R_{\mu 0}) \tag{9a}$$

where the sum over μ runs over all solvent sites, $\mathbf{R}_{\mu}$ represents the solvent site positions, $\mathbf{r}_0$ is the solute position, $R_{\mu 0} \equiv R_{\mu} - r_0$, $\hat{\mathbf{R}} \equiv \mathbf{R}/R$, $\Delta E(R_{\mu 0})$ is the solute−solvent energy gap, $\Delta E'(R_{\mu 0})$ is the derivative of ΔE with respect to $R_{\mu 0}$, and it is understood that the entire last expression is calculated as a nonequilibrium ensemble average. Equation 9a contains the same information as eq 7, but the sum over α in eq 7 is replaced by the sum over the solvent degrees of freedom $\mathbf{R}_{\mu}$ *plus* the solute degrees of

freedom ($\mathbf{r}_0$). In addition, it is straightforward to integrate any one of the projected nonequilibrium velocity response functions, $J_\alpha(t)$, back to a projected solvation response function, $S_\alpha(t)$; we have discussed the advantages of using the integrated projections in previous work.[15,34] We thus define the normalized nonequilibrium projection onto a degree of freedom α as

$$S_\alpha(t) = \frac{1}{2\lambda}\int_0^t \dot{\alpha}(t')\frac{\partial \Delta E(t')}{\partial \alpha}\,dt' = \frac{1}{2\lambda}\int_0^t \Delta \dot{E}_\alpha(t')\,dt' \equiv$$
$$\frac{1}{2\lambda}\int_0^t J_\alpha(t')\,dt' \quad (9b)$$

where $J_\alpha(t)$ is the solvation velocity projection onto the coordinate α from eq 7, λ is the solvent reorganization energy (eq 6), and like $J_\alpha(t)$, the integrands in the middle two expressions are calculated as nonequilibrium ensemble averages.

Unlike the equilibrium projections $C_{\alpha\beta}(t)$,[15] the projected $S_\alpha(t)$'s in eq 9b do not contain cross-coordinate terms. Thus, we take the second time derivative of ΔE to obtain the solvation acceleration response function, which is the closest nonequilibrium analogy to $G(t)$.[35] The total solvation acceleration response function, $B(t)$, is given by

$$-B(t) = \overline{\Delta \ddot{E}(R_{\mu 0};t)} = \frac{d}{dt}J(t) = \sum_\mu \frac{d}{dt}[\dot{\mathbf{R}}_{\mu 0}\cdot\hat{\mathbf{R}}_{\mu 0}\Delta E'(R_{\mu 0})] =$$

$$\sum_\mu \left\{ [\Delta E'(R_{\mu 0})\hat{\mathbf{R}}_{\mu 0}]\cdot\ddot{\mathbf{R}}_{\mu 0} + \left[\frac{\Delta E'(R_{\mu 0})}{R_{\mu 0}}\right] \times \right.$$

$$\left. \left|\dot{\mathbf{R}}_{\mu 0}\right|^2 - \dot{\mathbf{R}}_{\mu 0}\cdot\left[\hat{\mathbf{R}}_{\mu 0}\left(\frac{\Delta E'(R_{\mu 0})}{R_{\mu 0}} + \Delta E''(R_{\mu 0})\right)\hat{\mathbf{R}}_{\mu 0}\right]\cdot\dot{\mathbf{R}}_{\mu 0}\right\} \quad (10)$$

where, as with eq 9a, we have chosen to write the total $B(t)$ explicitly as a sum of the projections onto the solute and solvent center-of-mass Cartesian coordinates. In eq 10a, $\dot{\mathbf{R}}_{\mu 0} = \dot{\mathbf{R}}_\mu - \dot{\mathbf{r}}_0$ and $\ddot{\mathbf{R}}_{\mu 0} = \ddot{\mathbf{R}}_\mu - \ddot{\mathbf{r}}_0$ are the relative velocity and acceleration terms, and as with eq 9 the last two expressions are evaluated as nonequilibrium ensemble averages. We now define the normalized nonequilibrium projection onto any pair of scalar coordinates α and β, $S_{\alpha\beta}(t)$, by integrating twice,[15]

$$S_{\alpha\beta}(t) = \frac{1}{2\lambda}\int_0^t dt'\int_0^{t'} dt'' \left\{\left[\frac{\partial \Delta E}{\partial \alpha}\right]\ddot{\alpha} + \left[\frac{\partial \Delta E}{\partial \alpha}\right] \times \right.$$

$$\left. \left|\dot{\alpha}\right|^2 - \dot{\alpha}\left[\frac{\partial^2 \Delta E}{\partial \alpha \partial \beta}\right]\dot{\beta}\right\}$$

$$\equiv \frac{1}{2\lambda}\int_0^t dt'\int_0^{t'} dt'' \, B_{\alpha\beta}(t'') \quad (10b)$$

where $B_{\alpha\beta}(t)$ is the solvation acceleration response projected onto the coordinates α and β and the integrand in the second expression is calculated as a nonequilibrium ensemble average. Except where specifically noted, we will use the word "projection" to refer to the integrated projected solvation velocity or acceleration functions, eqs 9b and 10b.

In eqs 9a and 10a, the derivatives of the solvation energy gap contain the *relative* solute–solvent velocities and accelerations; this emphasizes that solvation dynamics is a cooperative effort involving motions of both the solute and solvent. In many simulations of solvation dynamics, however, the solute is chosen to be infinitely massive so that solute translations cannot participate in solvation dynamics. This approximation does have some physical grounding, because the solutes in many solvation experiments are large organic dyes that are 50 or 100 times more massive than the solvent molecules. In our simulations,
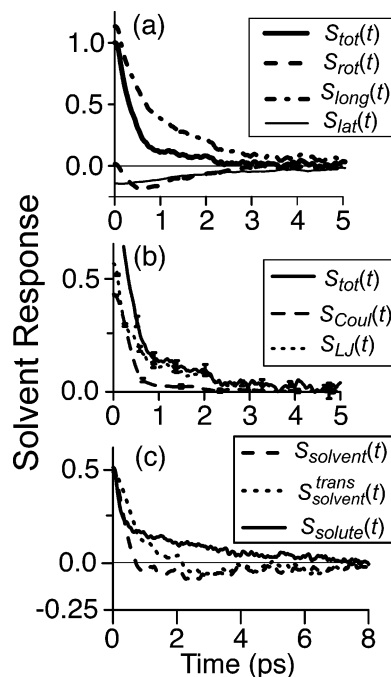
Figure 6. Projections (eq 9b) of the nonequilibrium solvation energy gap (averaged over all 400 nonequilibrium trajectories) for the reaction studied in Scheme 1. (a) shows the integrated projections for THF rotations ($S_{rot}(t)$, dashed curve), for solute–solvent center-of-mass longitudinal translations ($S_{long}(t)$, dash–dot curve), and for solute–solvent center-of-mass lateral translations ($S_{lat}(t)$, thin solid curve). (b) displays the projections onto the Coulomb ($S_{Coul}(t)$, dotted curve) and Lennard-Jones ($S_{LJ}(t)$, dotted curve) parts of the solute–solvent interaction. (c) shows the integrated projections onto motions of only the solvent ($S_{solvent}(t)$, dashed curve), only the solute ($S_{solute}(t)$, solid curve), and only the translational motions of the solvent ($S_{solvent}^{trans}(t)$, dotted curve). $S_{solvent}^{trans}(t)$ was calculated by subtracting the full rotational projection ($S_{rot}(t)$, (a)) from $S_{solvent}(t)$.[43] The total nonequilibrium solvent response function ($S_{tot}(t)$, eq 4, thick solid curve same as solid curve in Figure 3) is shown for comparison in (a) and (b). Note the scale changes on both axes in the different panels. In (a) and (c), the curves are calculated from eq 9b.[34] $S_{rot}(t)$ in (a) was calculated by subtracting $S_{long}(t)$ and $S_{lat}(t)$ from $S_{tot}(t)$.

however, the mass of our atomic solute is about one-third the mass of a solvent molecule, so we expect that solute translations will make an important contribution to the solvation dynamics.[36,37] Because the solvation dynamics in eqs 9a and 10a are projected onto relative solute and solvent motions, it is straightforward to separate the solute contributions to $\overline{\Delta E}$ from those of the solvent.[38] In the next section, we use projections to understand the nonequilibrium dynamics and the hidden breakdown of LR in these solute/THF systems.

B. Molecular Projections of Nonequilibrium Solvation Dynamics. Figure 6 summarizes various molecular projections of the nonequilibrium solvation dynamics for the reaction depicted in Scheme 1.[39] The thick solid curve in Figure 6a, $S_{tot}(t)$ (eq 1), is the calculated nonequilibrium solvent response function for the reaction depicted in Scheme 1, which is the same $S(t)$ shown in Figure 3. The dashed curve in Figure 6a shows $S_{rot}(t)$, defined as the sum of all three projections of the solvation energy gap onto solvent rotations (see inset to Figure 1); the dash–dot curve in Figure 6a shows $S_{long}(t)$, the projection of the solvation energy gap onto solute–solvent longitudinal center-of-mass translations (i.e., the direction between the solute and solvent's center of mass); and the thin solid curve shows $S_{lat}(t)$, the projection onto the two lateral, or transverse, translations (i.e., solute or solvent translations that do not change the solute–solvent center-of-mass distance). $S_{rot}(t)$ was calculated by

Molecular Projections of Solute and Solvent Motions

J. Phys. Chem. B, Vol. 107, No. 51, 2003 **14471**

subtracting $S_{trans}(t) = S_{long}(t) + S_{lat}(t)$ from $S_{tot}(t)$. The large contribution of center-of-mass longitudinal translations to the total solvation dynamics is as expected due to the large difference in the first solvent shell distances of the ground- and excited-state solute, as seen in the RDFs in Figure 4a.

Based on our reasoning in section III.B, the fact that longitudinal translational motions play an important role in the total solvent response is easy to understand. However, the behavior of the rotational projection comes as a surprise for several reasons. First, there is apparently a delayed onset of rotational coupling to the solvation energy gap; rotations make no contribution to the nonequilibrium solvation dynamics at early times. Second, the rotational projection shows two distinct relaxation regimes: an early-time regime ($t < \sim 700$ fs) with a negative slope, indicating that rotational motions cause a decrease of the solvation energy gap, followed by a slower regime ($t > \sim 700$ fs) with a positive slope, indicating that rotational motions at these times cause the solvation energy gap to become *larger*. This means that solvent rotational motions during the second regime either stabilize the unoccupied anion state or destabilize the newly created neutral solute (or both). The fact that a subset of the nonequilibrium solvent motions can work to increase the solvation energy gap whereas the rest work to lower it is highly counterintuitive, especially given that this type of effect cannot be present in equilibrium dynamics. Finally, at long times, the rotational projection contributes nothing to the overall change in the nonequilibrium energy gap, even though at intermediate times solvent rotations modulate the gap in a nontrivial way. We will return to the question of what causes this unusual behavior for solvent rotations below in section IV.C.

In addition to projecting the contributions of molecular motions, we can also explore how each portion of the pairwise solute−solvent interaction potential contributes to the nonequilibrium solvation energy gap by dividing the energy into Coulomb and Lennard-Jones (LJ) parts: $\overline{\Delta E} = \overline{\Delta E_{Coul}} + \overline{\Delta E_{LJ}}$.[40] The dashed curve in Figure 6b[41] shows the Lennard-Jones contribution to the solvent relaxation, $S_{LJ}(t)$, and the dotted curve shows the Coulomb contribution, $S_{Coul}(t)$. The Lennard-Jones projection shows relaxation on at least two distinct time scales: a rapid component at early times ($t < 400$ fs) and a slower contribution at longer times (0.5 ps $< t < 3$ ps), each with roughly equal amplitude. $S_{Coul}(t)$ shows a similar two-time scale behavior, although the rapid relaxation component accounts for $\sim 95\%$ of the Coulombic contribution of the solvent response. We note that analogous projections to these were presented in our previous work,[15] but the nonequilibrium average for the curves in Figure 6b was performed over twice as many trajectories.

Figure 6c shows the projections of the solvation energy gap onto the motions of just the solute or solvent, as suggested in section IV.A.[42] The figure shows clearly that solute motion is responsible for about half of the total relaxation dynamics.[36,37] Moreover, the total solvation response (solid curve) is fully relaxed by ~ 3 ps whereas both $S_{solvent}(t)$ and $S_{solute}(t)$ do not finish decaying for ~ 8 ps. This shows that solvation dynamics is a cooperative effort of the solute and solvent: the full solute−solvent system can relax faster than is possible with motions by either the solute or solvent alone. In fact, previous calculations have shown that the ratio of the solute and solvent masses can determine the rate of solvation,[36] emphasizing the important role of motions of the solute. Because for our atomic solute the full rotational projection ($S_{rot}(t)$ in Figure 6a) can arise only from the solvent, we subtracted this contribution from $S_{solvent}(t)$

to obtain the solvent-only translational projection, $S_{solvent}^{trans}(t)$, shown as the dotted curve in Figure 6c.[43] This curve makes it clear that the nonequilibrium translational motions of the solute and solvent contribute about equally to the total translational relaxation and thus to the total system relaxation (cf. Figure 6a). We also can identify the small negative portion of $S_{solvent}^{trans}(t)$ as coming from the lateral translations of the solvent (again cf. Figure 6a).

Next, we ask how the proximity of a particular solvent molecule to the solute determines its contribution to the solvation energy gap. Studies of other systems have shown that the solvation energy gap is modulated most strongly by the closest solvent molecule to the solute[14,36,44] or by a collective effort of the 6−12 solvent molecules in the first solvation shell.[45−47] To see how the nearby solvent molecules couple to $S(t)$ in our system, we calculated projections of $\overline{\Delta E}$ onto both nearest-neighbor and first-shell solvent molecules.[48] Because of diffusion, the locations of solvent molecules change during the nonequilibrium dynamics, so we calculated these projections using two different methods. In the first method, we determined the identity of the nearest neighbor (or first shell) molecule(s) at $t = 0$, and calculated the contribution of these molecules to the solvation gap throughout the trajectory (even if the molecule(s) diffuse away from the solute at later times). In the second method, the identity of the nearest neighbor (or first solvent shell) was updated at each time step, even if diffusional exchange switched the identity of the molecules. The two methods gave dramatically different results for the nearest-neighbor projection, which accounts for only $\sim 6\%$ of the total relaxation using the first method but over $\sim 20\%$ of the relaxation using the second. In contrast, we found little difference between the two methods for the projection onto the first-shell solvent molecules, both of which indicated that the first solvent shell is responsible for $\sim 80\%$ of the total relaxation.[49] This leaves longer-ranged Coulomb interactions from solvent molecules beyond the first solvent shell to account for the remaining $\sim 20\%$ of the total solvation dynamics.

C. Building a Microscopic Picture of Nonequilibrium Solvation Dynamics. How do all these different projections fit together to present a unified picture of the nonequilibrium solvation dynamics for this system? In the previous section, we showed that longitudinal center-of-mass translations of the nearby solvent molecules are responsible for most of the relaxation dynamics and that the lateral translations (which decayed on a separate time scale from the longitudinal translations) contributed very little to the total solvation dynamics. Figure 6a showed that the contribution from solvent rotations also has two components: a short-time process that decreases the solvation energy gap followed by a longer-time process during which the solvation energy gap increases. Moreover, the projection of $S(t)$ onto the LJ part of the solute−solvent interaction potential (Figure 6b, dashed curve) showed two different relaxation regimes. Finally, the bulk of the Coulomb projection (Figure 6b, dotted curve) relaxed on two more time scales. Although it is not immediately obvious how rotations and translations affect the solvation energy gap via the LJ and Coulomb interactions, it is clear that there are at least four different relaxation time scales: two rotational time scales plus one longitudinal and one lateral translational time scale from the projections in Figure 6a, or two Lennard-Jones and two Coulomb time scales from the energy projections in Figure 6b. These time scales must correspond to at least four different mechanisms for the nonequilibrium solvation dynamics. This
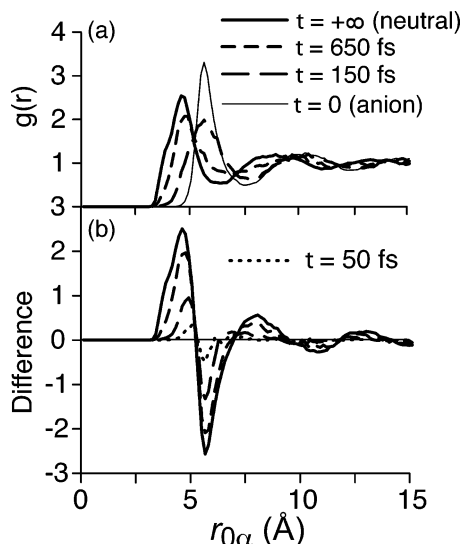
Figure 7. For the reaction of Scheme 1, (a) showing time-dependent nonequilibrium solute/solvent center-of-mass radial distribution functions (RDF) and (b) showing the differences between the ground-state (anion) RDF and the various time-dependent RDFs of (a). In both panels, the $t = 0$ (thin solid curves) RDF is calculated from the 200 ps equilibrium trajectory with the anionic (ground state) solute. Likewise, the $t = +\infty$ (thick solid curves) RDF is calculated from the 200 ps equilibrium trajectory with the neutral (excited state) solute. The remaining curves are calculated by averaging over the 400 nonequilibrium simulations. Each nonequilibrium RDF is calculated over a short (100 fs) block. For example, the $t = 650$ fs (dashed curves) RDF is the average RDF using the 600–700 fs block in each of the nonequilibrium trajectories. Note that for clarity we only show the $t = 50$ fs (dotted curve) difference curve in (b) and not the corresponding time-dependent RDF in (a). The peaks in (b) show where solvent density is increasing; the valleys in (b) show where solvent density is decreasing.

leads us to conclude that our nonequilibrium projections have uncovered at least four distinct underlying relaxation regimes.

To build a molecular picture of the motions underlying each of the distinct relaxation regimes, we have computed dynamic radial distribution functions (RDFs) to investigate how the local solvation structure changes with time following excitation. To calculate time-dependent RDFs, each nonequilibrium trajectory was broken into 100 fs segments, and the averaged RDF from each segment was then further averaged over the 400-trajectory ensemble; the results are shown in Figure 7a. Figure 7 also shows the equilibrium RDF for the excited-state solute (neutral, $t = +\infty$, thick solid curve). To make the structural changes clear, we also show the difference between the time-dependent RDFs and the equilibrium RDF for the ground-state solute (anion, $t = 0$, thin solid curve) in Figure 7b. The rising probability peak at ∼4.8 Å of panel b shows the influx of solvent molecules forming the first solvent shell around the newly created neutral solute, whereas the growing probability deficit at ∼5.2 Å shows the loss of the solvent structure imposed by the formerly occupied ground-state anion. Together, parts a and b of Figure 7 show that restructuring of the solvent around the smaller, neutral excited state is nearly complete after ∼650 fs; little additional rearrangement of the solvation structure takes place between 650 and 1150 fs (not shown). This allows us to assign the early-time (≤650 fs) portion of the translational relaxation to the rapid inward motion of the nearby solvent molecules, accounting for ∼50% of the total translational relaxation (cf. Figure 6a, $S_{\text{long}}(t)$ at $t = 650$ fs).

Figure 7 also makes it clear that the remainder of the nonequilibrium translational relaxation, which occurs on time scales longer than ∼650 fs, results from minor rearrangements
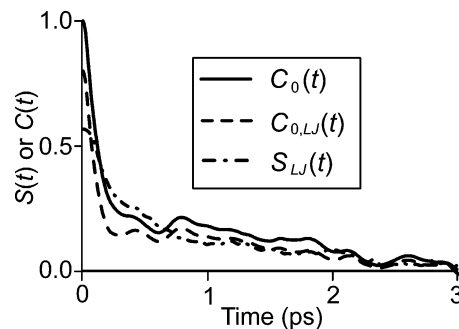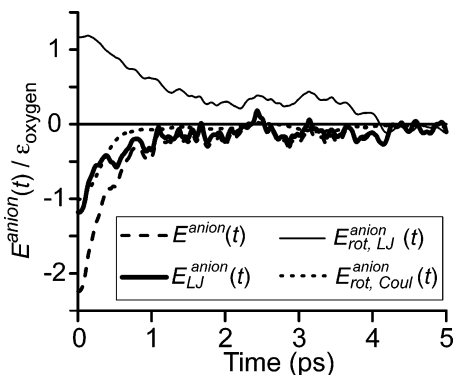

Figure 8. Projections of the nonequilibrium and equilibrium solvation response functions. $C_0(t)$ (solid curve, eq 2, same as dashed curve in Figure 3) is the equilibrium solvation response for the neutral solute (and the unoccupied excited state is the anion). $C_{0,\text{LJ}}(t)$ (dashed curve) is the Lennard-Jones projection of $C_0(t)$. $S_{\text{LJ}}(t)$ (dash−dot curve, same as dotted curve, Figure 6b) is the Lennard-Jones projection of the nonequilibrium response function. The agreement between $C_{0,\text{LJ}}(t)$ and $S_{\text{LJ}}(t)$ at long times ($t > \sim 1$ ps) is not coincidental; rather, it indicates that the dynamics fall within the limit of linear response; see text.

of the entire solvent structure. This larger scale repacking does not begin to take place until after (most of) the new first solvent shell structure is complete, so that the slower translational relaxation component occurs on diffusional time scales. We believe that the delayed onset of this long-time translational repacking results from the fact that the first solvent shell must translate inward before the second solvent shell can rearrange,[50] as documented in previous studies of solvation dynamics.[14,51,52]

Now that we see how translational solvent motions underlie the nonequilibrium relaxation, we can reconsider Figure 3, which showed that $C_0(t)$ and $S(t)$ look very similar at times longer than ∼1 ps. This similarity likely results from the fact that the final restructuring and fine-tuning of the solvent structure (including some of the first shell) in the nonequilibrium simulations lies within the LR approximation. By comparing the longitudinal (not shown) and Lennard-Jones projections for the equilibrium neutral simulations with those in Figure 6a,b, we find that the long-time ($t > 0.9$ ps) dynamics of $C_0(t)$ are nearly the same as the longitudinal and LJ projections in $S(t)$. Moreover, Figure 8 shows that the LJ projections of the long-time relaxation dynamics of $C_0(t)$ and $S(t)$ are virtually identical. This suggests that after ∼1 ps, the solute−solvent relaxation in the nonequilibrium simulations behaves as though the system is near equilibrium around the neutral solute. Thus, this long-time agreement is effectively in the linear response limit (and not a coincidence![15]).

Up to this point, we have seen that translations account for two of the four relaxation processes seen in the nonequilibrium solvation dynamics of this system (rapid translations that establish most of the neutral solvation structure and slower, diffusional translations that complete the solvation dynamics; Figures 6a and 7). The remaining two relaxation mechanisms result from solvent rotational motions. In section III.B we pointed out that modulation of the unoccupied state can contribute as much or more to the dynamics of the solvation energy gap as modulation of the occupied state. For the nonequilibrium simulations considered here, the destabilization of the (unoccupied) ground-state anion following excitation is ∼50 times larger than the stabilization of the (occupied) excited-state neutral. This means that we only need look at the dynamics of the energy of the unoccupied state, the anion−solvent interaction energy, $E^{\text{anion}}(t)$, to understand the nonequilibrium relaxation of the full solvation energy gap.[53] Consideration of only the anion solvation energy fits well with our arguments

Molecular Projections of Solute and Solvent Motions

J. Phys. Chem. B, Vol. 107, No. 51, 2003 **14473**

Figure 9. Nonequilibrium projections (eq 9b) of the un-normalized anion−solvent interaction energy as a function of time after excitation. The overall energy of the anion ($\overline{E^{\text{anion}}}(t)$, dashed curve) increases with time, thereby decreasing the total solvation energy gap ($\overline{E(t)}$). The Lennard-Jones ($\overline{E^{\text{anion}}_{\text{LJ}}}(t)$, solid curve) and Coulomb ($\overline{E^{\text{anion}}_{\text{Coul}}}(t)$, not shown) projections of the anion−solvent interaction energy are nearly the same as the corresponding projections of the total solvation energy gap in Figure 6b. $\overline{E^{\text{anion}}_{\text{Coul}}}(t)$ is not shown because the projection of Coulomb interactions onto solvent rotational motions ($\overline{E^{\text{anion}}_{\text{rot,Coul}}}(t)$, dotted curve) is nearly the same as $\overline{E^{\text{anion}}_{\text{Coul}}}(t)$. We assign these (Coulomb-based) rotational motions to the first of two distinct nonequilibrium relaxation mechanisms that come from solvent rotations (see text). The projection of LJ interactions onto first-shell solvent rotational motions ($\overline{E^{\text{anion}}_{\text{rot,LJ}}}(t)$, dash−dot curve)[56] shows a decrease of the energy of the anionic state. This means that the solvation energy gap is increasing with time and we assign this process to the second rotational relaxation mechanism (see text). All of these curves were calculated using a subset of only 49 of the nonequilibrium trajectories, and all of the rotational projections were calculated from eq 9b.[34]

that inward translation of the first-shell solvent molecules provides most of the relaxation of the gap: the solute−solvent translations that provide a slight stabilization of the neutral quickly lead to unfavorable interactions on the steep repulsive Lennard-Jones wall of the larger ground-state anion. In what follows, we will elucidate the contributions of solvent rotations to the nonequilibrium dynamics by investigating how rotational motions affect $\overline{E^{\text{anion}}}(t)$.

Figure 9 shows the total (un-normalized) energy of the unoccupied anion state, $\overline{E^{\text{anion}}}(t)$ (dashed curve). This curve is nearly identical to the relaxation of the total solvation energy gap, $S(t)$ (solid curve in Figure 3); the slight differences are due to the small changes in the solvation energy gap resulting from stabilization of the neutral. The various dotted and dashed curves in Figure 9 show different projections of the (un-normalized) energy of the unoccupied anion state; for clarity, all of the curves in Figure 9 have been shifted to asymptotically approach zero in the long-time limit. The figure shows that both the Lennard-Jones projection ($\overline{E^{\text{anion}}_{\text{LJ}}}(t)$, solid curve) and the Coulomb projection onto solvent rotations ($\overline{E^{\text{anion}}_{\text{rot,Coul}}}(t)$, dotted curve) destabilize the anion, resulting in a decrease of the solvation energy gap.[54,55] Moreover, $\overline{E^{\text{anion}}_{\text{rot,Coul}}}(t)$ increases on a time scale that matches well with the early-time stabilization of the solvation energy gap evident for $S_{\text{rot}}(t)$ (cf. Figure 6a, dashed curve). In contrast, the anion solvation energy is *stabilized* by rotational contributions of the anion−solvent Lennard-Jones interaction ($\overline{E^{\text{anion}}_{\text{rot,LJ}}}(t)$, dash−dot curve).[56] The rotational Lennard-Jones contribution ($\overline{E^{\text{anion}}_{\text{rot,LJ}}}(t)$) has a slower decay than $\overline{E^{\text{anion}}_{\text{rot,Coul}}}(t)$, so we assign the second rotational time

scale in Figure 6a to rotations by first-shell solvent molecules that increase the solvation energy gap via the LJ interaction.

How can we rationalize the fact that the LJ and Coulomb interactions resulting from first-shell rotational solvent motions not only have opposing effects on the solvation energy gap but also act on different time scales? In section III.A, we calculated equilibrium angular distributions around the ground- and excited-state solutes (Figure 5) and found that, on average, less than one more first-shell solvent dipole points toward the neutral solute than points toward the anionic solute.[33] Thus, the solvent rotational motions that matter most to ΔE must be those that (on average) move the negatively charged oxygen site on the one "anomalous" first-shell solvent molecule closer to the anion (i.e., the THF dipole rotates from pointing "away" to pointing "towards" the solute, as per the convention in Figure 5b). As soon as this rotational motion begins, the unfavorable Coulomb interaction with the oxygen site should destabilize the anionic solute and thus decrease the solvation energy gap. This destabilization acts rapidly because only small rotations of the dipole are necessary to decrease the gap, so we assign the early-time rotational relaxation mechanism to this rapid rotational motion that destabilizes the anion state via the Coulomb interaction.

After causing the early-time destabilization of the anion solvation energy, however, the anomalous THF molecule continues to rotate, and the end result is an increase in the number of THF oxygen sites pointing toward the solute. Indeed, in section III.A, we calculated the solute-oxygen RDFs and found that the THF oxygen−solute distance decreases more than the THF center-of-mass-solute distance (cf. Table 2 and Figure 4b). This increase in the number of proximal THF oxygen sites comes at the expense of having to move THF methylene sites away from the solute. Because the THF oxygen-site LJ size parameter is ~1 Å smaller than the corresponding methylene-site size parameter (cf. Table 1), the long-term result of solvent rotations is to replace larger solvent sites near the solute with smaller solvent sites. This produces a decrease of (part of) the Lennard-Jones interaction energy with the unoccupied anion state, thereby increasing the solvation energy gap. In combination, Figures 5a and 7 show that rotational motions have no net effect on the solvation energy gap: the rotations first quickly destabilize the anion via the Coulomb interaction, but on a longer time scale, rotations lead to Lennard-Jones interactions with smaller solvent sites that provide a roughly equal amount of stabilization.

It is important to remember that these solvent rotations work to solvate the small neutral excited state and are not driven in any way by the unoccupied anionic ground state. The fact that rotational motions cause smaller sites to interact with the neutral and also result in a slight decrease in the energy of the unoccupied anion is coincidental. However, because the overall energy of the anion state increases so dramatically, this small effect (of opening the energy gap) is not observed without the method of projections presented in section IV.A and ref 15.

V. Conclusions

In summary, we have calculated many of the important equilibrium and nonequilibrium dynamical properties of Jorgensen's model of liquid THF. We found that all of the rotational and translational degrees of freedom in THF relax on similar time scales. We also studied the nonequilibrium solvation dynamics resulting from the removal of charge from an anionic atomic solute in THF. Because the time scales for translational and rotational relaxation are similar, we had to

project the solvation energy gap onto various molecular motions to uncover how specific degrees of freedom contributed to the solvation dynamics. In combination, the results led to a picture in which the bulk of the relaxation was caused by relative translations of the solute and solvent. The initial translational relaxation resulted from rapid solute−solvent translations due to the size decrease of the solute upon excitation. The longer-time translational relaxation was due to a subtle, whole-system, repacking on diffusional time scales. We also found an unusual cancellation in the solvent rotational projections that led to no net change in the solvation energy gap; early-time rotational motions rapidly decreased the gap via the Coulomb interaction, but the solvation energy gap was also slowly increased via favorable Lennard-Jones interactions between the anionic solute and the smaller oxygen site on THF.

With the molecular picture summarized above, we are now in a position to understand the reason for the breakdown of LR in this system, and why (without projection analysis) the breakdown is hidden. LR breaks down because the excited-state solute allows the solvent to sample a different configuration phase space than the ground state: due to its larger size, the ground-state anion prevents the solvent from modulating the solvation energy gap at distances between 3.3 and 4.2 Å (cf. Figure 7). Because this is a region around the excited-state neutral that has an appreciable density of solvent molecules, LR cannot possibly be a valid approximation for this system. The coincidental agreement between $S(t)$ and $C_−(t)$ in Figure 3 stems from the fact that the rotational and translational motions of THF occur on similar time scales, as seen in Figure 2. This means that no matter how the different translational and rotational motions couple to the energy gap, the equilibrium and nonequilibrium solvent response functions will tend to decay on similar time scales.

Finally, we close by reiterating that this work was motivated by femtosecond experiments of the charge-transfer-to-solvent reaction of the sodium anion in THF being performed in our lab.[7] In particular, our experimental work indicates that detachment of electrons from sodium anions in THF takes approximately 700 fs. If the model for THF that we have employed here is accurate, then the 600−700 fs time scale for translational solvation by THF could suggest that translational motions are responsible for detachment in CTTS reactions.[7] Work is currently underway in our group to implement both one-[57] and two-electron[58] mixed-quantum/classical simulations of the CTTS reaction with sodide in this model of THF to build a molecular-level understanding of the pump−probe experiments that motivated this work.

References and Notes

(1) Chandrasekhar, J.; Jorgensen, W. L. *J. Chem. Phys.* **1982**, *77* (10), 5073.

(2) Chandrasekhar, J.; Jorgensen, W. L. *J. Chem. Phys.* **1982**, *77* (10), 5080.

(3) Drabowicz, *W. Z Naturforsch. A.* **1990**, *45* (11−12) 1342.

(4) Bareman, J. P.; Reid, R. I.; Hrymak; A. N.; Kavassalis, T. A. *Mol. Simul. 11* (2−4) 243.

(5) Helfrich, J.; Hentschke, R. *Macromolecules* **1995**, *11* (28), 3831.

(6) (a) Girard, S.; Müller-Plathe *Mol. Phys.* **2003**, *101* (6), 779. (b) Faller, R.; Schmitz, H.; Biermann, O.; Müller-Plathe, F *J. Comput. Chem.* **1999**, *20*, 1009.

(7) (a) Barthel, E. R.; Martini, I. B.; Schwartz, B. J *J. Chem. Phys.* **2000**, *112* (21), 9433. (b) Martini, I. B.; Barthel, E. R.; Schwartz, B. J *J. Chem. Phys.* **2000**, *113* (24), 11245. (c) Barthel, E. R.; Martini, I. B.; Schwartz, B. J. *J. Phys. Chem. B* **2001**, *105* (49) 11230. (d) Martini, I. B.; Barthel, E. R.; Schwartz, B. J. *J. Am. Chem. Soc.* **2002**, *124* (25), 7622. (e) Barthel, E. R.; Martini, I. B.; Keszei, E.; Schwartz, B. J. *J. Chem. Phys.* **2003**, *118*, 5916. (f) Barthel, E. R.; Schwartz, B. J. *Chem. Phys. Lett.* **2003**, *375* (3−4), 435.

(8) Maroncelli, M. *J. Mol. Liq.* **1993**, *57*, 1.

(9) (a) Rosenthal, S. J.; Jimenez, R.; Fleming, G. R.; Kumar, P. V.; Maroncelli, M. *J. Mol. Liq.* **1994**, *60*, 25. (b) Schwartz, B. J.; Rossky, P. R. *J. Phys. Chem.* **1995**, *99*, (10), 2953.

(10) Mukamel, S. *Principles of Nonlinear Optical Spectroscopy*; Oxford: New York, 1995. Cho, M.; Yu, J.-Y.; Joo, T.; Nagasawa, Y.; Passino, S. A.; Fleming, G. R. *J. Phys. Chem.* **1996**, *100*, 11944.

(11) Chandler, D. *Introduction to Modern Statistical Mechanics*; Oxford University Press: New York, 1987.

(12) See, e.g.: Ma, J.; Vanden Bout, D. A.; Berg, M. *J. Chem. Phys.* **1995**, *103*, 9146.

(13) (a) Skaf, M. S.; Ladanyi, B. M. *J. Phys. Chem.* **1996**, *100*, 18258. (b) Day, T. J. F.; Patey, G. N. *J. Chem. Phys.* **1999**, *110*, 10937. (c) Laria, D.; Skaf, M. S. *J. Chem. Phys.* **1999**, *111*, 300.

(14) (a) Aherne, D.; Tran, V.; Schwartz, B. J. *J. Phys. Chem. B* **2000**, *104* (22), 5382. (b) Tran, V. and Schwartz, B. J. *J. Phys. Chem. B* **1999**, *103* (26), 5570−80.

(15) Bedard-Hearn, M. J.; Larsen, R. E.; Schwartz, B. J. *J. Phys. Chem. A* **2003**, *107* (24), 4773.

(16) (a) Ladanyi, B. M.; Maroncelli, M. *J. Chem. Phys.* **1998**, *109* (8), 3204. (b) Ladanyi, B. M.; Stratt. R. M. *J. Phys. Chem. A* **1998**, *102*, 1068.

(17) Ladanyi, B. M.; Perng, B.-C. *J. Phys. Chem. A* **2002**, *106*, 6922.

(18) Steele, W. A. *Mol. Phys.* **1987**, *61* (4), 1031.

(19) Allen, M. P.; Tildesely, D. J. *Computer Simulation of Liquids*; Oxford University Press: New York, 1987.

(20) Ciccotti, G.; Ferrario, M.; Ryckaert, J.-P. *Mol. Phys.* **1982**, *47* (6), 1253.

(21) Steinhauser, O. *Mol. Phys.* **1982** *45* (2), 335.

(22) The tapering function was employed only for the actual molecular dynamics, and was not used in the computation of ΔE in the solvation dynamics calculations.

(23) Dawes, S. B.; Ward, D. L.; Fussa-Rydel, O.; Huang, R.-H.; Dye, J. L. *Inorg. Chem.* **1989**, *28*, 2132.

(24) Pyper, N. C.; Pike, C. G.; Edwards, P. P. *J. Am. Chem. Soc.* **1993**, *115*, 1468.

(25) We picked starting configurations for the nonequilibrium trajectories from the ground-state (anion) equilibrium trajectory. The starting configurations had an average separation of ∼1 ps, with a minimum separation of 0.5 ps.

(26) Because there are two possible tumbling directions, a $\hat{\mathbf{u}}_{t1}$, $\hat{\mathbf{u}}_{t2}$ cross term arises, which is of the form $\psi_{t1,t2}(t) = \langle \hat{\mathbf{u}}_{t1}(t) \cdot \hat{\mathbf{u}}_{t2}(0) \rangle + \langle \hat{\mathbf{u}}_{t2}(t) \cdot \hat{\mathbf{u}}_{t1}(0) \rangle$.

(27) Relaxation times are sometimes defined as $\tau = \int_0^\infty \psi(t)$; using this definition, we find very similar results for the tumbling and spinning decay rates. $\tau_{tumble} = 1.9$ ps and $\tau_{spin} = 1.7$ ps

(28) Stratt, R. M.; Jang, J. *J. Chem. Phys.* **2000**, *112* (17).

(29) (a) Anderson, J.; Ullo, J.; Yip, S. *J. Chem. Phys.* **1987**, *86* (7), 4078. (b) Chelli, R.; Cardini, G.; Procacci, P.; Righini, R.; Califano, S.; Albrecht, A. *J. Chem. Phys.* **2000**, *113* (16), 6851. (c) Chelli, R.; Cardini, Ricci, M.; Bartolini, P.; Righini, R.; Califano, S. *Phys. Chem. Chem. Phys.* **2001**, *3*, 2803.

(30) Error bars shown are 2 standard deviations. For both of the autocorrelation functions, we calculated the error bars by breaking up the 200 ps equilibrium simulations into 127 separate 10 ps blocks with each starting point separated by 1.5 ps. These blocks were then correlated as per eq 2 and averaged.

(31) Yan, Y. J.; Mukamel, S. *J. Chem. Phys.* **1988**, *89*, 5160.

(32) Hansen, J.-P.; McDonald, I. R. *Theory of Simple Liquids*, 2nd ed.; Academic Press Ltd.: San Diego, CA, 1990.

(33) On the basis of the solute−solvent center-of-mass RDFs in Figure 4a, we defined the first solvent shell for the neutral and anionic solutes as all THF molecules residing within 6.5 and 7.5 Å, respectively, the values of the minima after the first peak in the RDF. For Figure 5, we defined the first-shell molecules as those within 7.5 Å, regardless of the nature of the solute. This means that the two angular distributions each contain ∼12 solvent molecules, even though the first shell around the neutral (using the 6.5 Å definition) only contains 8−9 molecules.

(34) When integrating $J_\alpha(t)$ (we used a simple midpoint integration algorithm), there is a linear term that must be subtracted from each of the integrated projections to obtain the curves similar to those in Figure 3. This is done by fitting the tail (in our case, the last 5 ps) of the integrated projection to a line and then subtracting that line from the integrated function. The fitting must be done in the tail of the curve at times after the solvation

dynamics are complete; that is, where the average $S_\alpha(t)$ is known to be zero. When integrating $B_{\alpha\beta}(t)$ (eq 10b), there is a quadratic term that should be just as easily removed as the linear term in the integrated $J_\alpha(t)$, but our statistics did not allow us to fit this accurately enough to integrate $B_{\alpha\beta}(t)$.

(35) $B(t)$ is the closest analogy to $G(t)$, but the two functions have different units; $[B(t)]$ = energy/time^2, whereas $[G(t)]$ = energy^2/time^2. This is one reason it is necessary to integrate the projected functions to compare to the full $S(t)$ or $C(t)$. As discussed in our previous Letter,[15] it is also advantageous to integrate to obtain information about the magnitude of the coupling for a particular degree of freedom.

(36) Larsen, R. E.; David, E. F.; Goodyear, G.; Stratt, R. M. *J. Chem. Phys.* **1997**, *107* (2), 524.

(37) Roy, S.; Bagchi, B. *Chem. Phys.* **1994**, *183*, 207.

(38) This separation can be done directly using eqs 9a and 9b, whereas the use of eqs 10a and 10b would result in solute−solvent cross terms.

(39) The projections of $S(t)$ in Parts a and c of Figure 6 were calculated with eq 9b; we are justified in using eq 9b rather than eq 10b because we previously determined that the magnitude of the translation/rotation cross term is negligible for this system.[15] Our choice to use the solvation velocity response function, $J(t)$, is based on high noise levels in the acceleration response function, $B(t)$; the second derivative function $B(t)$ varies too rapidly and our 400 nonequilibrium trajectories did not provide sufficient statistics to accurately integrate $B(t)$ twice (as in eq 10b).

(40) Nitzan, A.; Graf, P. *Chem. Phys.* **1998**, *235*, 297.

(41) The curves in Figure 6b did not require using either eq 9b or 10b, because it is trivial to substitute $\overline{\Delta E} = \overline{\Delta E_{\text{Coul}}} + \overline{\Delta E_{\text{LJ}}}$ directly into eq 1.

(42) Admittedly, this projection of the solute and solvent coordinates onto the stationary lab frame is arbitrary because only relative separations matter for solvation dynamics. We could have just as easily chosen to project the solvation dynamics in a reference frame that moves along with the solute particle.

(43) We note that calculating the projection directly and integrating would have given the exact same curve, because the analysis using eqs 9a and 9b does not contain cross terms.

(44) Ladanyi, B. M.; Stratt, R. M. *J. Phys. Chem.* **1995**, *99*, (9), 2502.

(45) Perera, L.; Berkowitz, M. *J. Chem. Phys.* **1992**, *96* (4), 3093.

(46) Chang, S. L, Wu, T.-M. *Chem. Phys. Lett.* **2000**, *324*, 381.

(47) Kuharski, R. A.; Bader, J. S.; Chandler, D.; Sprik, M.; Klein, M. L.; Impey, R. W. *J. Chem. Phys.* **1988**, *89*, 3248; Bader, J. S.; Chandler, D. *J. Phys. Chem.* **1992**, *96*, 6423.

(48) These projections onto the first-shell and nearest neighbor molecules are not integrated. They were computed directly by selecting the appropriate subset of molecules in the nonequilibrium average for $S(t)$, eq 1.

(49) Figure 4a shows that the first solvent shell around the anion is both farther away (7.5 Å) than the neutral (6.5 Å) and contains more solvent molecules (12−13) than the neutral (8−9). We performed the nonequilibrium solute first-shell projections both for molecules within 6.5 and for molecules within 7.5 Å; this change of the first-shell definition only changed its contribution by ∼1 or 2%.

(50) In fact, due to packing constraints, some of the anion's first-shell solvent molecules need to translate out to become part of the second solvent shell around the neutral.

(51) Onsager, L. *Can. J. Chem.* **1977**, *55*, 1819.

(52) However, solvation for this system occurs in the opposite manner to Onsager's famous "inverse snowball" (ref 51). See, for example: (a) ref 45. (b) Papazyan, A.; Maroncelli, M. *J. Chem. Phys.* **1993**, *98* (8), 6431. (c) Fonseca, T.; Ladanyi, B. M. *J. Phys. Chem.* **1991**, *95*, (6) 2116.

(53) Even though we will examine only the unoccupied anion state to describe the nonequilibrium solvation dynamics, the dynamics are driven only by the neutral solvent−solvent interactions. That is, modulation of the anion energy by solute or solvent motions is motivated not by the anion but by the new interactions with the now-occupied neutral state.

(54) The rotational Coulomb projection is nearly identical to $S_{\text{Coul}}(t)$ (cf. Figure 6b, dotted curve) and $E_{\text{Coul}}^{\text{anion}}$ (not shown).

(55) The translational projections onto the anion solvation energy (not shown) are nearly identical to the translational projections of the total solvation energy gap shown in Figure 6a.

(56) The rotational projection of the LJ energy for the anion state ($E_{\text{rot,LJ}}^{\text{anion}}(t)$ dash−dot curve, Figure 8) results solely from first-shell solvent rotations because the LJ potential is so short-ranged.

(57) Smallwood, C. J. Bosma, W.; Larsen, R. E.; Schwartz, B. J. *J. Chem. Phys.* **2003**, *119*, 11263.

(58) Larsen, R. E.; Schwartz, B. J. *J. Chem. Phys.* **2003**, *119*, 7672.